Cepero-Mejías, F., Curiel-Sosa, J.L., Zhang, C., Phadnis, V.A. Effect of cutter geometry on machining induced damage in orthogonal cutting of UD polymer composites: FE study. Composite Structures, 214, pp. 439-450 (2019).

Effect of cutter geometry on machining induced damage in orthogonal cutting of UD polymer composites: FE study

Cepero-Mejías F.[a,b,c,*], Curiel-Sosa J. L.[b,c], Zhang C.[d], Phadnis V. A.[e]

[a]*Industrial Doctorate Centre in Machining Science, The University of Sheffield, Sir Frederick Mappin Building, Mappin Street, S1 3JD Sheffield, United Kingdom.*
[b]*Computer-Aided Aerospace & Mechanical Engineering (CA2M) Research Group, Sir Frederick Mappin Building, Mappin Street, S1 3JD Sheffield, United Kingdom.*
[c]*Department of Mechanical Engineering, The University of Sheffield, Sir Frederick Mappin Building, Mappin Street, S1 3JD Sheffield, United Kingdom.*
[d]*School of Mechanical Engineering, Jiangsu University, Zhenjiang, China*
[e]*AMRC with Boeing, Advanced Manufacturing Park, Wallis Way, Catcliff, Rotherham, S605TZ, United Kingdom.*

Abstract

This article presents a finite-element analysis (FEA) based study to understand the influence of cutting parameters (rake angle, relief angle and cutter edge radius) on the machining-induced damage of unidirectional (UD) composites. Carbon/epoxy (CFRP) and glass/epoxy (GFRP) composites are considered. Onset of damage in composites is modelled using a combination of maximum stress and Puck's fracture criteria, while a novel damage propagation algorithm is proposed to account for the post-damage material softening behaviour. A spring-back phenomenon (partial elastic recovery of workpiece material after tool passed a cutting surface) often observed in composites machining, is considered in the FE model to allow a better prediction of the thrust force and induced damage. A validated FE model predicts that with increasing relief angle, the extent of sub-surface damage is reduced. Rake angle or tool edge radius are not found to have a great influence on the induced damage. A large dependence is observed between the fibre angle and the induced damage, as the severity of damage increase when fibre orientations varies from 30° to 90°.

Keywords: Machining, Induced machining damage, Finite element, Modelling, Orthogonal cutting, Composite

1. Introduction

In the last decade, the use of polymer matrix composites (PMCs) has become widespread due to their superior properties. PMCs are often manufactured to a near-net shape, though require finish

*Corresponding author.
Email addresses: `fmcepero1@sheffield.ac.uk` (Cepero-Mejías F.), `j.curiel-sosa@sheffield.ac.uk` (Curiel-Sosa J. L.), `zhangchao@ujs.edu.cn` (Zhang C.), `v.phadnis@sheffield.ac.uk` (Phadnis V. A.)
URL: `https://www.ms-idc.co.uk/meet-students` (Cepero-Mejías F.), `https://www.sheffield.ac.uk/mecheng/staff/jcurielsosa` (Curiel-Sosa J. L.)

cutting operations to remove excess material and achieve strict assembly tolerances. Machining PMCs is typically challenging owing to intrinsic properties of its constituents. During machining, tougher polymer resins and hard fibres could cause excessive mechanical stress on the cutting edge, while low thermal conductivity of resins bypasses the majority of process heat to a cutting tool, resulting in accelerated wear. Consequently, blunt cutting tools with unfavourable cutting parameters bend fibres ahead of the cutting tool tip rather than shearing them away [1, 2]. This thermo-mechanical abuse gives rise to a variety of damage modes in PMCs such as fibre/resin pull-out, resin thermal-degradation and delamination [3–5]. The resultant damage sites, in turn, could affect the surface quality of a machined component and act as potential crack nucleation sites when loaded in service [6].

A large number of cutting trials are generally needed to fully characterise machining responses (typically, cutting forces, cut surface quality, surface and sub-surface damage and tool wear) of a particular combination of a fibre/matrix system and cutting tool geometry. This could be a cumbersome and very costly venture. Numerical models of machining accounting for appropriate material constitutional relationships, underlying physics and validated using experimental data can be a great virtual alternative in such cases.

Analytical models predicting composites machining responses are primarily limited to calculations of critical force responsible for delamination initiation in drilling applications [7], and tool wear on the simplified tool geometries. Several underpinning complexities such as heterogeneity of thermo-mechanical properties of PMCs, complex cutter geometries and dynamic friction changes in high-speed machining, as well as high strain rate-effects limit the use of analytical models. FE models on the other hand, though, are not computationally as economical, pose a viable option to study all above mentioned parameters in depth.

Various length-scale approaches (micro-, meso- and macro-scale) are used to model machining response of composites depending upon the motivation of the study. For example, micro-scale FE models simulating orthogonal cutting of composites [8–12] allow prediction of machining damage to individual fibre/matrix constituents as well as fibre-matrix de-bonding. These computational analyses can provide fairly accurate information on localised damage, though are complex and computationally expensive for the amount of the information that can be extracted. Macro-scale FE models, on the other hand, consider use of homogenised material properties. A variety of fibre/matrix damage modes and their interactions can be simulated using advanced mathematical criteria accounting for fracture and damage mechanics [13–15]. Cohesive zone modelling (CZM) approach is also popular amongst researchers to model interply delamination [16].

A limited number of studies incorporating a full 3D FE model of composite machining are available to date, and mostly focussed at predicting interply delamination in orthogonal cutting application [17–20], mainly due to the extent of computational resources needed. Consequently, majority of published FE models consider 2D plane stress approximation [21–28] to analyse influence of cutting parameters on the subsurface damage. Few interesting studies and their outcomes are briefed next. Santiuste et al. [21] developed a 2D FE model of orthogonal cutting to demonstrate that the subsurface damage was much reduced in machining brittle (CFRP) composites than in ductile (GFRP) composites. They further developed a 3D model of the same process accounting for thermal effects [29] the model though accounts for cutting force prediction and chip formation successfully, fails to consider interaction of thermal degradation of resin properties and the overall workpiece stiffness reduction due to mechanical damage. In another study aimed at understanding influence of cutting parameters on the machining response of composites, Zenia et al. [22] identified fibre orientation, rake angle and depth of cut as critical factors affecting cutting forces and induced damage. It was suggested that increase in the depth of cut could lead to higher cutting forces and induced damage, while increase in rake angle reduce the same. Soldani et al. [23] also considered the effect of cutting edge radius along with other cutter geometry parameters, and concluded that the use of a sharper tool edge radius can reduce the subsurface damage significantly. A critical review of these state-of-the-art FE models suggests that though these could be used to predict machining response terms of induced damage, chip morphology, and cutting forces; data used in their validation is often very limited. For example, most of the published FE models studying composites machining are validated by comparing numerically predicted cutting forces with the experimental data [30–32], though an extent of machining induced damage is usually not measured for a validation purpose.

In the current work, a 2D FE model of orthogonal cutting of UD CFRP composite is presented. It accounts for the effect of various cutting parameters - cutter rake and relief angle, cutting edge radius and fibre orientation- on machining induced damage of composites. FE model employ a combination of maximum stress and Pucks fracture criteria to model damage initiation based on critical stress value, while post-damage material softening is accounted for using an energy-based approach. Mechanics for material spring-back is also considered. FE models are validated using experimental cutting force data as well as optical measurements of machining induced damage [24].

2. Model characteristics

Several 2D FEM plane stress quasi-static analysis are performed with the numerical software package Abaqus/Explicit. Positive fibre orientations of 0°, 15°, 30°, 45°, 60°, 75° and 90° are assessed in this work. A standard cutting configuration coherent with parameters used for Bhatnagar et al. [24] in their experiments is considered to validate the numerical results. Fig. 1 shows an schematic illustration of cutting parameters treated ahead.

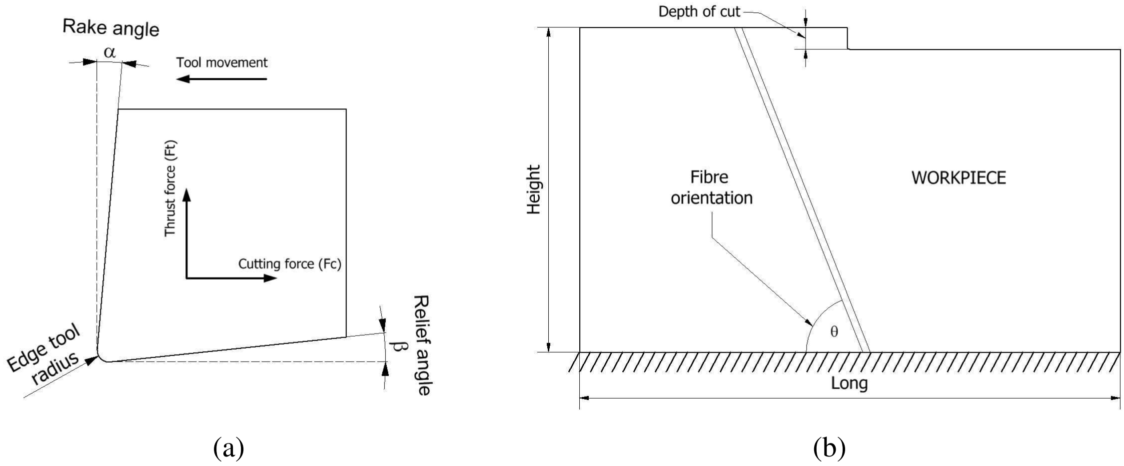

Fig. 1. (a) Tool and (b) workpiece cutting parameters.

2.1. Machining configurations and geometric analysis

To evaluate the induced damage influence of rake angle, relief angles, tool edge radius and workpiece material ten cutting configurations are simulated. The desired cutting variable studied is changed to keep the rest of cutting variables the same values with the standard configuration. In Table 1 a representation of all cutting variables values examined in this work is offered.

Table 1
Cutting variables employed in this work

Cutting variables	Standard configuration	Cutting variables values studied
Rake angle (α)	5°	-5°, 0°, 10°
Relief angle (β)	6°	4°, 8°, 10°
Tool edge radius (μm)	50	30, 15
Depth of cut (mm)	0.2	-
Workpiece material	GFRP	CFRP
Cutting speed (mm/s)	8.33	-

A 5 mm long and 3 mm height workpiece are investigated. As a boundary condition, workpiece bottom side is fixed while for lateral sides the horizontal displacement is restricted as shown in Fig. 2. Elastic and strength properties of UD-GFRP and UD-CFRP used in this work are extracted from the Santiuste et al. [21] and Phadnis et al. [16] publications, respectively. Table 2 and Table 3 collects the elastic and strength properties of the studied UD-GFRP and UD-CFRP composites.

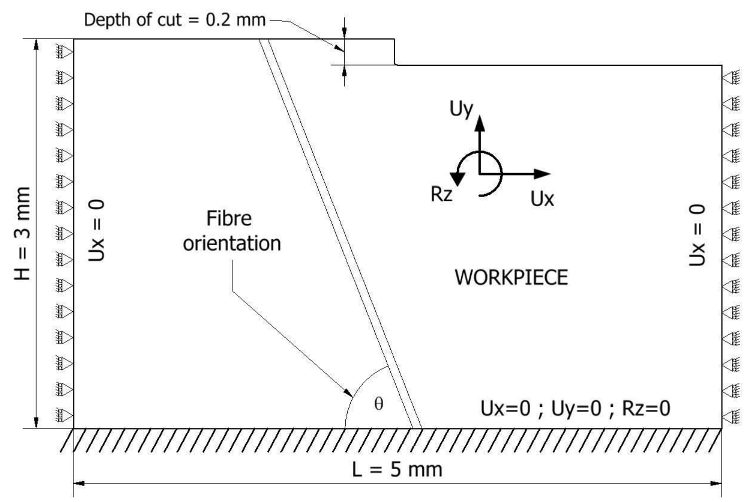

Fig. 2. Workpiece boundary conditions.

Table 2
Elastic properties of GFRP and CFRP materials used in this work

Material	$E_{11}(GPa)$	$E_{22}(GPa)$	$G_{12}(GPa)$	υ_{12}
GFRP [21]	48	12	6	0.28
CFRP [16]	136.6	9.6	5.2	0.29

Table 3
Strength properties of GFRP and CFRP materials used in this work

Material	$X_T(MPa)$	$X_C(MPa)$	$Y_T(MPa)$	$Y_C(MPa)$	$S(MPa)$
GFRP [21]	1200	800	59	128	25
CFRP [16]	2720	1690	111	214	115

2.2. Meshing parameters

Quadrilateral elements with linear interpolation and reduced integration (CPS4R) are selected. Deletion of elements is not considered in this work. Besides, the low cutting speed applied in the simulation make the FEM analysis could be considered as a quasi-static problem. This issue allows increasing the composite density while the model kinematic energy stands in low values without affecting the final results. In this model, density is increased using an appropriate mass scaling factor until achieving an integration time of around 10^{-8} and 10^{-9} s.

Mesh element size is selected to reach a right time-accuracy combination. A rectangular zone next to the cutting tool meshed with a medium element size of 10 μm. The remaining area is more coarsely mesh using partitions which increase the element size progressively from the 10 μm in the refined mesh vicinity until achieving the value of 100 μm in the outer edges. These partitions avoid the excessive element distortion and improve the numerical results quality (refer to Fig. 3).

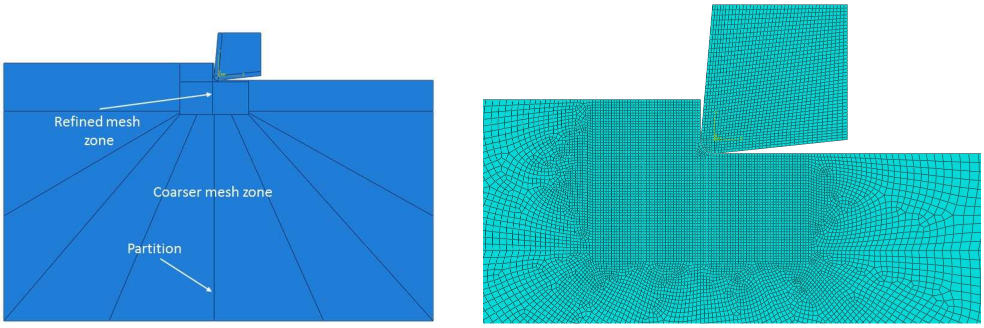

(a) (b)

Fig. 3. (a) Mesh distribution and (b) Zoom of the refined mesh area.

2.3. Contact and friction modelling

The tool is considered as a solid rigid body. The contact between the tool and the workpiece is performed with a surface-node surface contact property. A constant Coulomb friction coefficient of 0.2 is employed in all simulations. This is not the best method to model the contact, because the friction coefficient should vary with the fibre orientation. However, because of the lack of information in this matter, other authors have been using this methodology for simulating the tool-workpiece friction [21, 22, 25].

3. FEM damage algorithm basics

The new proposed damage algorithm was implemented in Abaqus/explicit through a user subroutine VUMAT. Constitutive equations considered in this work are extracted from the damage model proposed by Lapczyk and Hurtado [33]. In this formulation, four different damage modes are present: fibre traction (d_{ft}), fibre compression (d_{fc}), matrix traction (d_{mt}) and matrix compression (d_{mc}). Hereafter, the combination of these damage modes inside stiffness matrix is showcased in Eq. (1).

$$\begin{bmatrix} \sigma_{11} \\ \sigma_{22} \\ \sigma_{12} \end{bmatrix} = \begin{bmatrix} (1-d_f)E_{11} & (1-d_f)(1-d_m)\nu_{21}E_{11} & 0 \\ (1-d_f)(1-d_m)\nu_{12}E_{22} & (1-d_m)E_{22} & 0 \\ 0 & 0 & (1-d_s)G_{12} \end{bmatrix} \begin{bmatrix} \varepsilon_{11} \\ \varepsilon_{22} \\ \varepsilon_{12} \end{bmatrix} \tag{1}$$

$$, where\ D = 1-(1-d_f)(1-d_m)\nu_{12}\nu_{21} \quad ; \quad d_s = 1-(1-d_{ft})(1-d_{fc})(1-d_{mt})(1-d_{mc})$$

$$d_f = max\{d_{ft}, d_{fc}\}\ ;\ d_m = max\{d_{mt}, d_{mc}\}\ ;\ d_I \epsilon [0,1]\ and\ I = (ft, fc, mt, mc)$$

Because of composite brittle behaviour matrix plasticity is not taken into account. In addition, isothermal conditions are contemplated in this work for simplicity. Composites material behaviour is modelled with an initial linear elastic response until damage initiation took place. The maximum stress failure criterion is selected to determine the fibre damage initiation, while for the matrix the Puck plane stress failure criterion is chosen. Five distinct damage modes are considered, fibre traction, fibre compression, matrix mode A, matrix mode B and matrix mode C.

Equations to reach the fibre traction and fibre compression damage initiation criteria are represented in Eqs. (2) and (3).

- Fibre traction ($\sigma_{11} > 0$)

$$F_{ft} = \left(\frac{\sigma_{11}}{X_T}\right) \geq 1 \tag{2}$$

- Fibre compression ($\sigma_{11} < 0$)

$$F_{fc} = \mid \frac{\sigma_{11}}{X_C} \mid \geq 1 \tag{3}$$

Where F_{ft} *and* F_{fc} represents the fibre traction and compression damage activation functions, respectively. Henceforth, these damage activation functions are named only activation functions for simplicity. Plane stress failure Puck criteria modes are chosen because it offers good matrix failure predictions in comparison with other extended composites failure criteria [34]. In this document, the basics of this failure are provided. For completion, a brief explanation of the Puck matrix failure modes variables is given. Interested reader is referred to [35] for a more detailed information.

Matrix plane stress Puck failure criteria are composed of three failure modes: (1) Mode A, (2) Mode B and (3) Mode C. In Mode A matrix rupture is occasioned under traction conditions, while Mode B and Mode C are taken place under normal compressive stresses. Mode A and Mode B cut the laminate in parallel with thickness direction while Mode C split the laminate with a certain angle. Puck matrix failure modes predictions contain a high level of complexity as appreciated in Eqs. (4) to (6).

F_{mma}, F_{mmb} and F_{mmc} represents the Mode A, Mode B and Mode C damage activation functions, respectively. To clarify the analysis of results only a matrix traction activation function (F_{mt}) and matrix compression activation function (F_{mc}) are analysed. Value of (F_{mt}) is assigned to be the same than F_{mma}, while (F_{mc}) is established as the maximum of F_{mmb} and F_{mmc} in every element ($F_{mc} = max\{F_{mmb}, F_{mmc}\}$).

Matrix traction activation function ($F_{mt} = F_{mma}$)

- Matrix Mode A ($\sigma_{22} \geq 0$)

$$F_{mma} = \sqrt{\left(\frac{\sigma_{12}}{R^A_{\perp\parallel}}\right)^2 + \left(1 - \frac{p^{(+)}_{\perp\parallel}}{R^A_{\perp\parallel}} R^{(+)A}_{\perp}\right)^2 \left(\frac{\sigma_{22}}{R^{(+)A}_{\perp}}\right)^2} + \frac{p^{(+)}_{\perp\parallel}}{R^A_{\perp\parallel}} \sigma_{22} \geq 1 \tag{4}$$

Matrix compression activation function ($F_{mc} = max\{F_{mmb}, F_{mmc}\}$)

- Matrix Mode B ($\sigma_{22} < 0$ *and* $\sigma_{22} > -R^A_{\perp\perp}$)

$$F_{mmb} = \sqrt{\left(\frac{\sigma_{12}}{R^A_{\perp\parallel}}\right)^2 + \left(\frac{p}{R}\right)^2 \sigma_{22}^2} + \left(\frac{p}{R}\right) \sigma_{22} \geq 1 \tag{5}$$

- Matrix Mode C ($\sigma_{22} \leq -R^A_{\perp\perp}$)

$$F_{mmc} = \frac{1}{2\left[1 + \left(\frac{p}{R}\right) R^A_{\perp\perp}\right]} \left[\left(\frac{\sigma_{12}}{R^A_{\perp\|}}\right)^2 + \left(\frac{\sigma_{22}}{R^A_{\perp\perp}}\right)^2\right] \frac{R^A_{\perp\perp}}{-\sigma_{22}} \geq 1 \tag{6}$$

Here, all terms with R represent the strength components associated with the fracture plane. Term $R^{(+)A}_{\perp}$ is equal to the transverse matrix traction strength (Y_T), $R^A_{\perp\|}$ corresponds to the intralaminar shear strength (S_{12}). Variable $R^A_{\perp\perp}$ is the transverse/transverse shear strength and generally this variable is quite difficult to measure, so the value is normally extracted indirectly from Eq. (7). Term $p^{(+)}_{\perp\|}$ is the Puck failure envelope slope when $\sigma_{22} > 0$ at point $\sigma_{22} = 0$. Recommendable values for this variable are 0.35 for carbon fibre composites and 0.3 for glass fibre composites [36]. Expression $\left(\frac{p}{R}\right)$ is calculated using the equation formulated in Eq. (8).

$$R^A_{\perp\perp} = \frac{Y_C}{2\left(1 + p^{(-)}_{\perp\perp}\right)} \tag{7}$$

$$\left(\frac{p}{R}\right) = \frac{p^{(-)}_{\perp\|}}{R^A_{\perp\|}} \tag{8}$$

In the above equations, values recommended for the variables $p^{(-)}_{\perp\perp}$ and $p^{(-)}_{\perp\|}$ are 0.3 for carbon fibre composites and 0.25 for glass fibre composites [36].

After damage onset is achieved, a linear continuum damage mechanics (CDM) approach is performed. The expression used to calculate the damage modes quantity in every step is shown in Eq. (9).

$$d_I = \frac{\delta^f_{I,eq}\left(\delta_{I,eq} - \delta^0_{I,eq}\right)}{\delta_{I,eq}\left(\delta^f_{I,eq} - \delta^0_{I,eq}\right)} \quad (d_I \in [0,1] \; and \; I = (ft, fc, mt, mc)) \tag{9}$$

Final ($\delta^f_{I,eq}$) and initial ($\delta^0_{I,eq}$) equivalent displacements are calculated immediately after the damage initiation condition of one damage mode is reached. These terms are determined by Eq. (10) and Eq. (11), respectively. Fracture toughness values show in Table 4 are employed in the present work.

Table 4
Critical fracture toughness extracted from [37]

N/mm	G^c_{ft}	G^c_{fc}	G^c_{mt}	G^c_{mc}
Critical fracture toughness	10	10	1	1

$$\delta^f_{I,eq} = \frac{2G^c_I F_I}{\sigma_{I,eq}} \tag{10}$$

$$\delta^0_{I,eq} = \frac{\delta_{I,eq}}{F_I} \tag{11}$$

In the above equations, coefficient F_I with $I = (ft, fc, mt, mc)$ represents the activation function value of the correspondent damage mode. $\sigma_{I,eq}$ and $\delta_{I,eq}$ are the equivalent stress and displacements of a damage mode, respectively. Expressions assigned to obtain the value of these variables are explained in detail in Ref. [33].

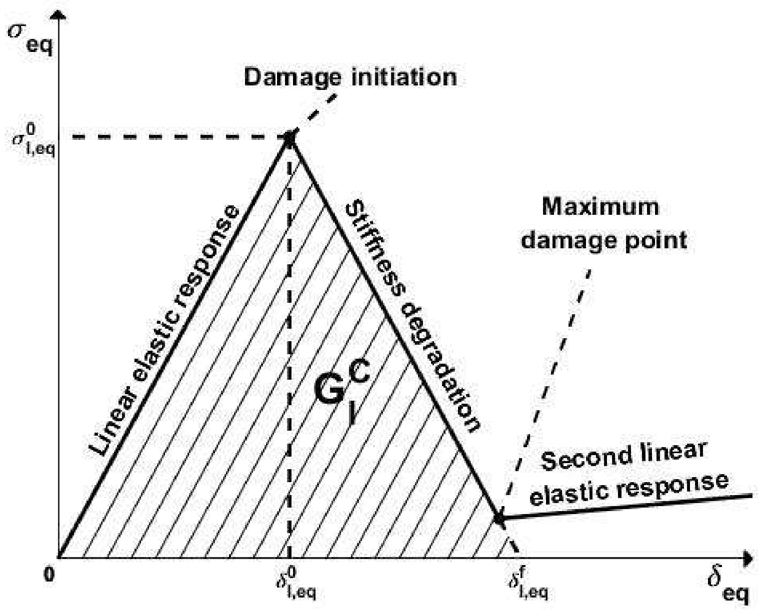

Fig. 4. Damage model scheme carried out for every damage mode.

Finally, maximum damage of 0.95 is allowed for the matrix and 0.999 for the fibre damage modes. These maximum values are chosen to avoid numerical errors [25] and simulate the remaining stiffness that a total failure ply supply to adjacent laminate plies [36]. After this damage level was achieved a second linear elastic response is introduced with the remaining stiffness. An illustration of the material behaviour scheme carried out is represented in Fig. 4.

4. Model validation

The standard cutting configuration model is validated by comparison with the experimental results obtained by Bhatnagar et al. [24]. The chip is assumed to be formed when the simulated cutting force reaches the experimental values obtained. Cutting and thrust forces are registered until the chip formation process was accomplished. Maximum cutting and thrust forces simulated are chosen as the machining forces to analyse the numerical results.

This assumption is considered reasonable, because of the non-deletion of elements carried out in the simulations avoid the apparition of the natural machining forces fluctuations [25]. An example of one simulation records of the cutting and thrust forces is provided in Fig. 5.

Spring back phenomenon, which consider the partial laminate thickness recovery that always takes place after the tool pass away (Fig. 5), is taken to improve the numerical damage predictions. This concept is introduced, imposing a linear progressive vertical penetration to the tool, while it is advancing horizontally; final vertical displacements for every fibre orientations are chosen in the order of the half or one tool edge radius value as studied by Wang et al. [38] and they are showcased in Table 5. This approach is developed to avoid the excessive meshed elements distortion under the tool that take place when only vertical displacement is applied. The real depth of cut considered is 0.2 mm, while to calculate the nominal depth of cut the vertical tool penetration should be added, see Table 5.

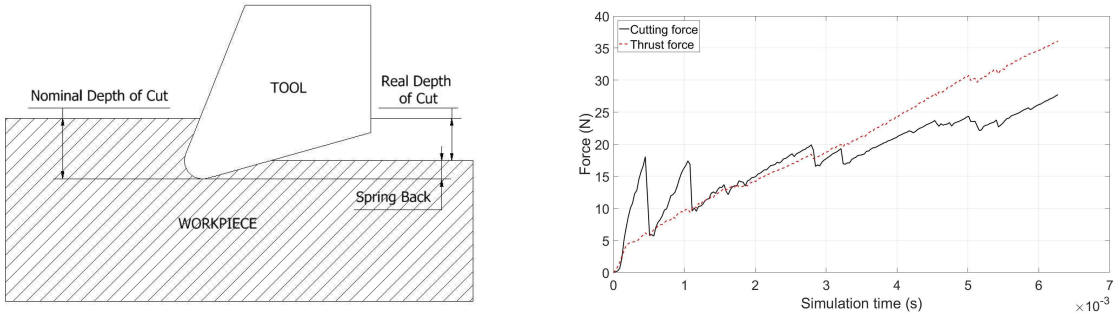

(a) (b)

Fig. 5. (a) Spring back phenomen representation and (b) example of machining forces record for the simulation of the standard cutting configuration and a fibre orientation of 0°.

Lasri et al. [25] and Santiuste et al. [21] validated their simulations using the cutting force obtained in Bhatnagar et al. [24] experiments. However, thrust force is poorly predicted as a result of not including the spring back phenomenon effects on composite machining response. This work proves the importance of this phenomenon on thrust force enhancing previous numerical predictions, as shown in Fig. 5.

In addition, the machining sub-surface damage is assessed through the activation functions (F_{ft}, F_{fc}, F_{mt} *and* F_{mc}) introduced previously. Sub-surface damage is assumed to be the vertical distance between the lowest element where it is equalised or exceeded the damage initiation condition and the machining trim surface. In this work the damage initiation condition is achieved after reaching or exceed F_{mt} and F_{fc} a value of 0.75 or F_{mc} and F_{ft} a value of 1. This decision is taken because fibre experience buckling problems in compression states and matrix have properties degradation problems in traction states [36]. Therefore, it is decided to be conservative with fibre compression and matrix traction damage modes.

Table 5
Vertical speed, cutting tool displacements and simulation time obtained for every fibre orientation simulating the standard cutting configuration

Fibre orientation	0°	15°	30°	45°	60°	75°	90°
Vertical penetration (mm)	0.0313	0.0226	0.0411	0.0395	0.0407	0.0439	0.0600
Nominal depth of cut (mm)	0.2313	0.2226	0.2411	0.2395	0.2407	0.2439	0.2600
Horizontal displacement (mm)	0.0521	0.0236	0.0381	0.0366	0.0679	0.1465	0.3202
Simulation time (s)	0.0063	0.0029	0.0046	0.0044	0.0082	0.0176	0.0394

From the results is obtained that fibre damage initiation criterion is not reached in low laminate locations. Hence, the matrix damage modes determine the sub-surface damage in all simulations. In Fig. 7 the evolution of matrix damage modes and shear and transverse stresses in different laminate areas is assessed, see Fig. 7. Three distinct matrix induced damage modes are distinguished in different workpiece positions: (1) beneath, (2) behind and (3) in front of the tool.

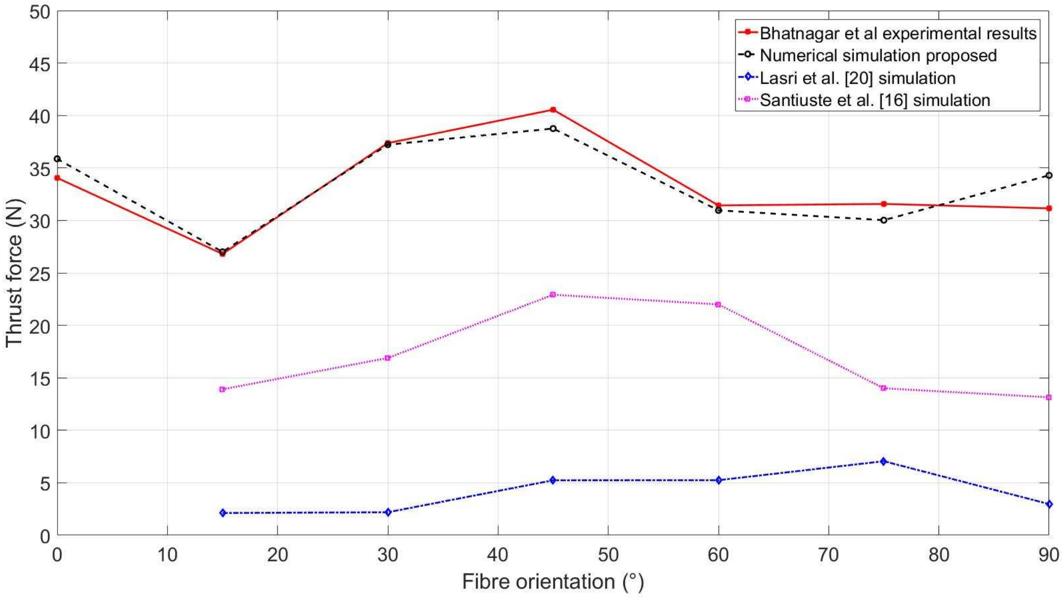

Fig. 6. Thrust forces obtained in the proposed numerical simulation and other publications.

As shown in Fig. 7(d), d_{mt} is found behind, while d_{mc} occurs in front positions as illustrated in Fig. 7(e). Both matrix damage modes are obtained in low laminate positions (Fig. 7(c)). For clarification, failure allocations in Puck's failure envelope is provided in Fig. 7(f). Main reasons to obtain these results are:

- Zone 1: Shear stresses are predominat, allocating the failure point in the boundary between traction and compression failure modes.
- Zone 2: Important traction transverse stresses are obtained because the pulling effect of the tool tip produce a Mode A or matrix traction failure.

- Zone 3: Mode C or matrix compression damage is detected due to the high compressive transverse stresses produced by the pushing action of the tool.

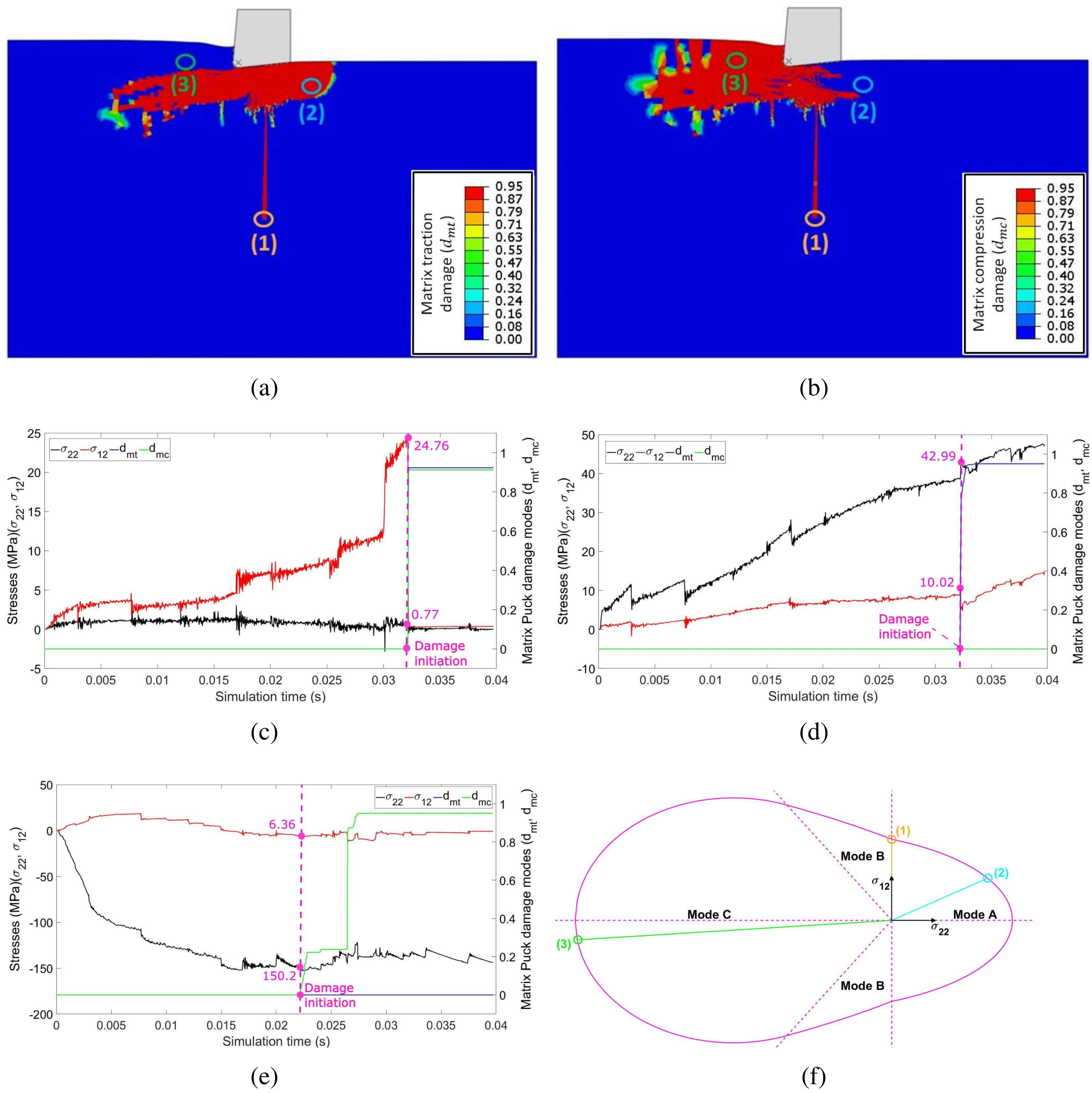

Fig. 7. Detailed illustrations of the matrix damage modes causes at final simulation time with the standard configuration and a fibre orientation of 90°: (a) Matrix traction damage (d_{mt}), (b) Matrix compression damage d_{mc}, (c), (d), (e) σ_{22}, σ_{12}, d_{mt} and d_{mc} predicted in position (1), (2) and (3), respectively and (f) Damage modes allocation using the Puck's matrix failure criterion in different laminate positions

Finally, the maximum sub-surface damage measured in the simulations achieved a significant improvement in comparison with Bhatnagar et al. [24] results, as depicted in Fig. 8. For all fibre orientations excepting 90° the predicted values are closer to experimental ones than the Bhatnagar's predictions achieved.

This fact could be solved with the inclusion of matrix plastic deformation; it would increase the energy required to move the tool and increment the sub-surface damage predictions. Besides, the fibre/matrix debonding has a relevant role for high fibre orientations 60-90°; this fibre bending effect would increase appreciably the predicted damage depth, especially for a fibre orientation of 90°. This factor is not included in this work, the development of a micro mechanical FE model should be required to analyse these particular cases to obtain more accurate predictions. However, the influence of cutter geometries on the induced damage is still affordable with this numerical model as both numerical and experimental results follow the same trend.

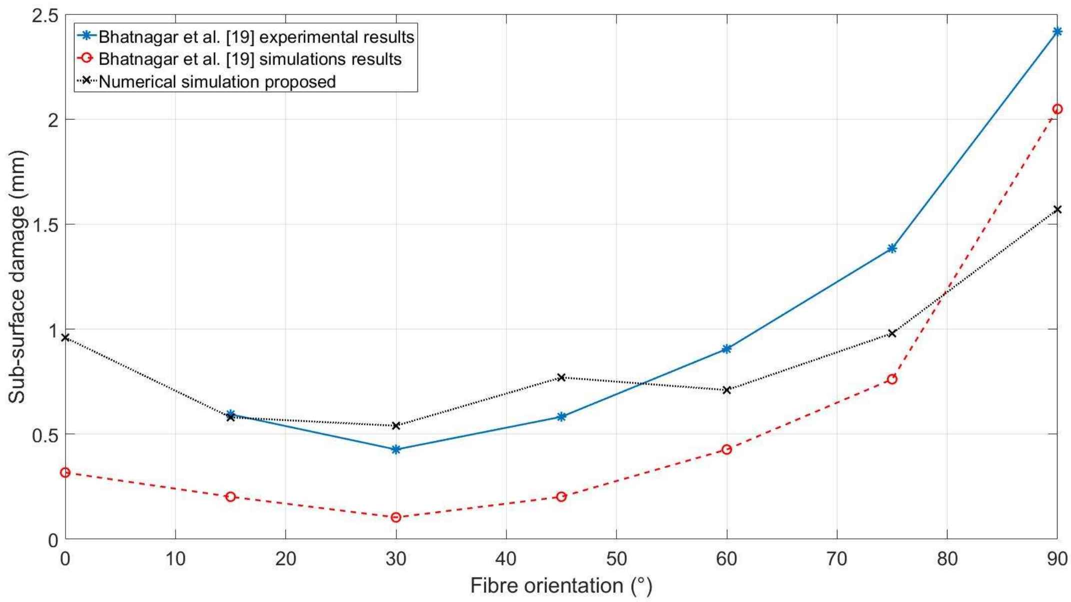

Fig. 8. Sub-surface damage obtained in the numerical simulation proposed and Bhatnagar et al. [24] numerical and experimental results

5. Results and discussion

Main contributions in this article are summarized in this section. For all simulations performed only one of the desired cutting parameters is changed, keeping the rest with the standard configuration values (refer to Table 1). In order to compare the influence of cutting parameters on the induced machining damage, ten cutting configurations are assessed. They are performed applying the same tool displacement and velocities used for the standard cutting configuration (refer to Table 5).

5.1. Fibre orientation influence

In this work, the damage activation function is used to reflect the predicted sub-surface damage area accounting the initial damage conditions exposed in section 3 ($F_{mt} = 1$ or $F_{mc} \geq 0.75$). Therefore, these variables not only point the damage areas, but also indicate the laminate zones where damage is close to occur and residual stresses might be found. Henceforth, for brevity purpose, only F_{mt} or F_{mc} will be shown in every section as both functions predicts similar sub-surface damages below the tool, as explained in section 4.

Fig. 8 shows the induced damage contours for different fiber orientations. It can be seen that the induced damage is highly dependant on the fiber orientation. In general, the damage area is mainly propagated in parallel and perpendicular fibre direction as represented in Fig. 9.

Lower induced damages are achieved for 15° and 30° fibre orientations, while higher values are obtained for 75° and 90°. The implication of high tool-workpiece contact stiffness for low fibre orientations produced a fragile chip rupture without excessive damage propagation. For a fibre orientation of 0° the fibre buckling effects are detected, introducing unstable effects on damage propagation.

For higher fibre orientations the tool-workpiece contact stiffness is mainly governed by the matrix; thereby it is softer than the contact produces with low fibre orientations. Due to this fact, a significant energy increment is required to achieve the chip generation. As a result, the sub-surface damage extension is deeper for these unidirectional composite laminates. Lastly, for a fibre of 90° a fine line of the sub-surface in the thickness direction is appreciated. This finding reveals a significant fibre-matrix debonding which increase the damage extension because the tool pushed the fibre away.

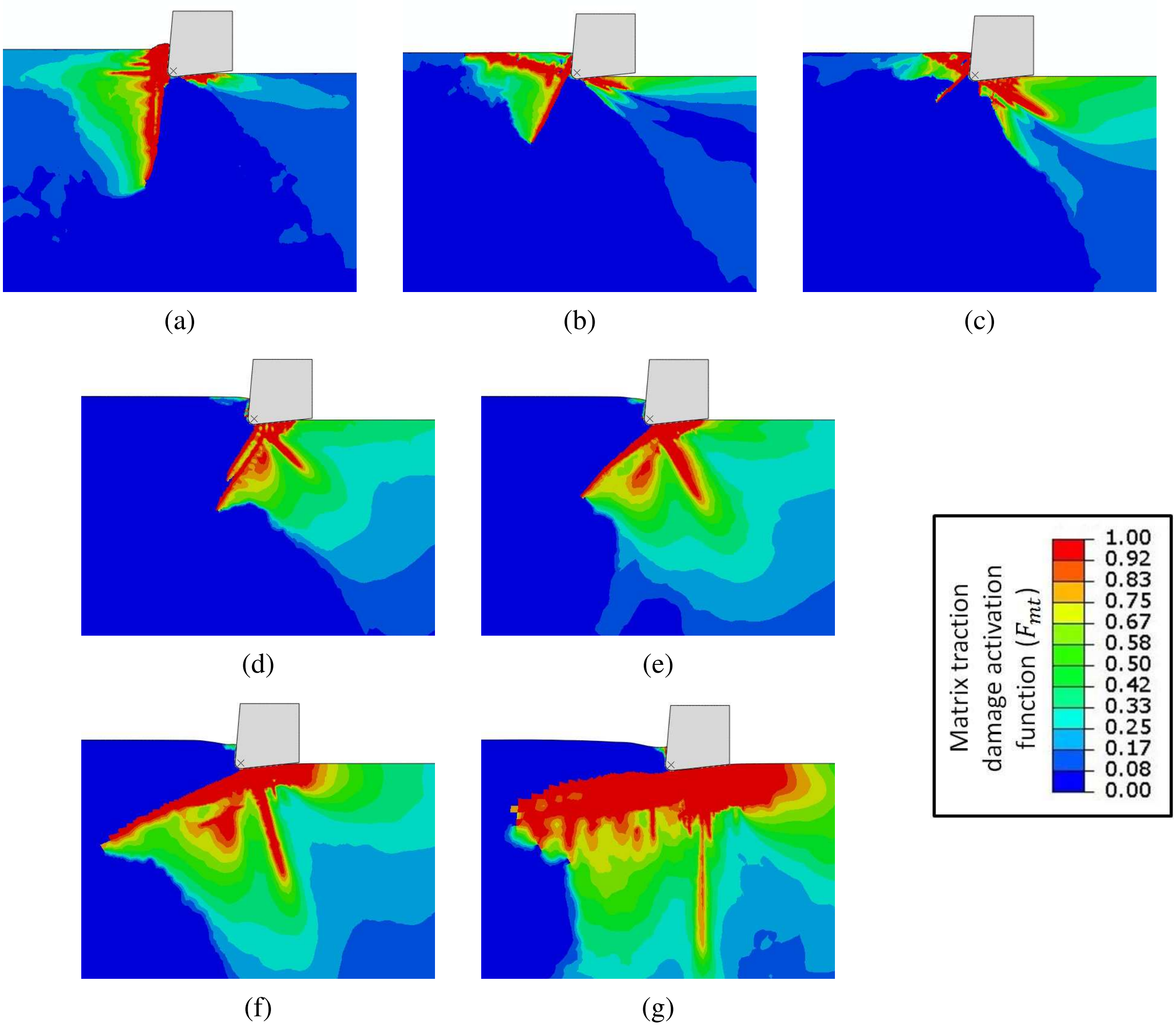

Fig. 9. F_{mt} obtained for fibre orientations (a) 0° (b) 15°, (c) 30°, (d) 45°, (e) 60°, (e) 75° and 90° at final simulation time with the standard cutting configuration.

5.2. Workpiece material influence

UD-CFRP and UD-GFRP composites are simulated to assess the influence of different material properties. It is found that levels of induced damage are significantly lower for UD-CFRP in all fibre orientations, see Fig. 11. In the case of UD-CFRP composites, a fragile damage behaviour is appreciated while UD-GFRP laminates shows a ductile behaviour. This behaviour is explained because of the higher contact stiffness properties between the tool and UD-CFRP composites.

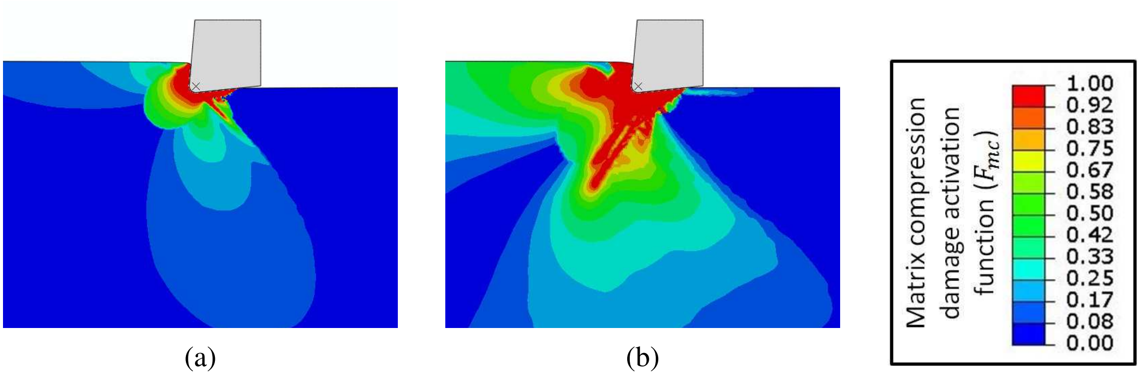

Fig. 10. F_{mc} illustration of (a) UD-CFRP composites and (b) UD-GFRP composites at final simulation time and fibre orientation of 45°.

The UD-GFRP composites increased more than 144.83% the machined induced damage simulated in UD-CFRP composites. For most fibre orientations the UD-GFRP composites sub-surface damage exceeded the 200% or even the 300% the damage obtained for UD-CFRP composites; reaching the maximum difference of a 375.76% for fibre orientation of 90°. Hence, it is concluded that CFRP composites are better materials to machine than GFRP composites in terms of induced machining damage response. An illustration of the matrix compression damage area (F_{mc}) for both materials with a fibre orientation of 45° is presented in Fig. 10.

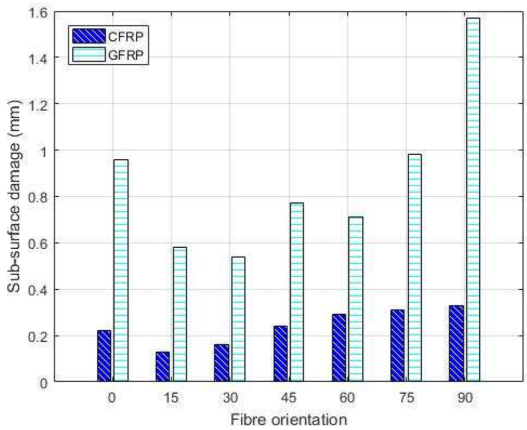

Fig. 11. Sub-surface damage obtained for all the workpiece materials and fibre orientations studied at the final simulation time.

Note that, because of the high stiffness of CFRP composites the machining peak forces are substantially incremented in comparison with GFRP composites, as show in Fig. 12.

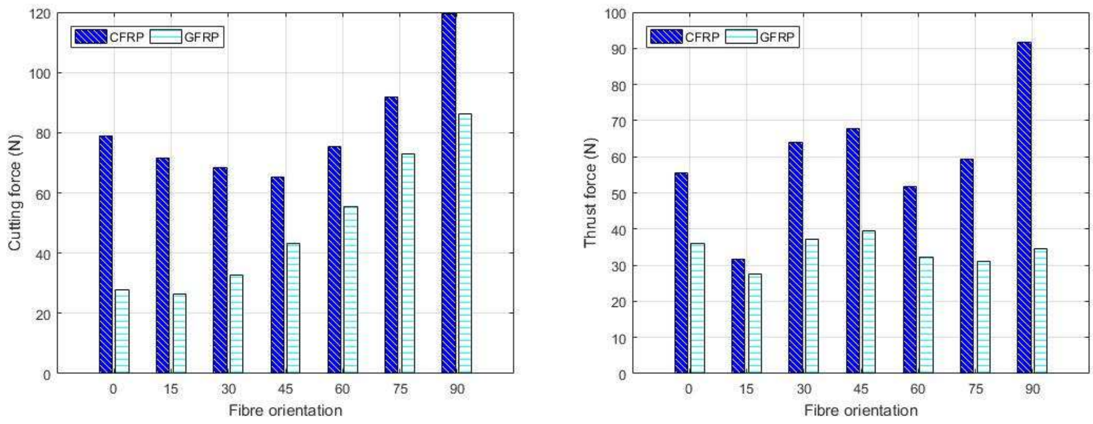

(a) (b)

Fig. 12. (a) Cutting and (b) thrust forces obtained for all the workpiece materials and fibre orientations studied at the final simulation time.

5.3. *Tool edge radius influence*

In Fig. 13 the induced damages obtained with the 15 μm, 30 μm and 50 μm edge tool radius simulated are plotted. This increment of edge tool radius chosen is simulated to observe the effects on the laminate damage that tool wears cause. An edge radius of 15 μm represents the geometry of a new cutting tool faithfully. Whereas, radius of 30 μm and 50 μm model the increased edge radius of the cutting tools after several machining operations.

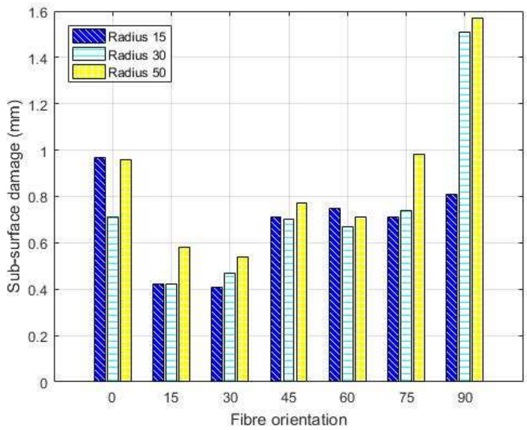

Fig. 13. Sub-surface damage obtained for all the tool edge radius and fibre orientations studied at the final simulation time.

For fibre orientations of 15° and 75° tool edge radius 15μm and 30 μm reduce the sub-surface damage extension obtained with a tool edge radius of 50 μm. For 30°, 45° and 60° fibre orientations, the tool edge radius influence on the subsurface damage is observed to be negligible in the studied radius range.

In the case of 0°, a significant damage reduction is obtained with a tool edge radius of 30 μm. This damage reduction is not realistic and it is reached due to the behaviour of laminates with fibre orientations of 0 degrees is especially difficult to model; in this case, fibres are parallel to the tool movement providing a rigid tool-workpiece contact making the internal damage propagation unstable introducing significant numerical errors. For a fibre orientation of 90°, the use of a low tool edge radius is found to be highly recommended to reduce the laminate damage area significantly, see Fig. 14.

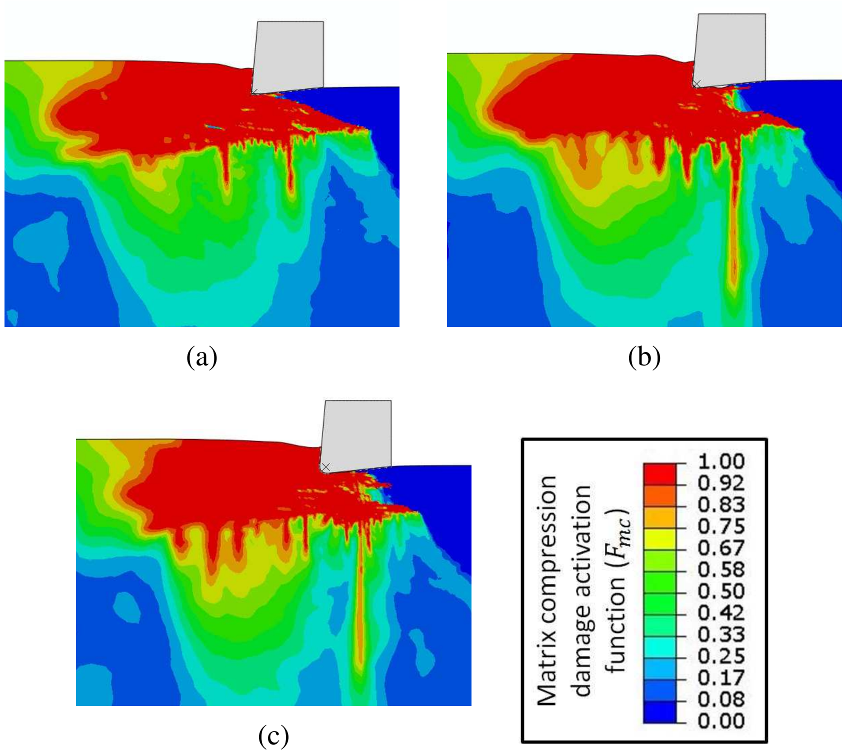

Fig. 14. F_{mc} obtained for tool edge radius of (a) 15 μm (b) 30 μm, (c) 50 μm at final simulation time for a fibre orientation of 90°.

It is concluded that lower tool edge radius produce better machining surfaces than cutting tools with higher edges radius. However, the maximum sub-surface damage increment is observed small (below the 40%) for fibre orientations between 0° and 75°. Hence, it is determined that the tool wear until 50 μm does not increase the sub-surface damage critically for fibre orientations between 0° and 75°.

5.4. Relief angle influence

Machining configurations with 4°, 6°, 8° and 10° are analysed, see Fig. 15. In general terms, the use of higher relief angles is beneficial to minimise the sub-surface damage as shown in Fig. 15(a). Same tendency is appreciated for thrust forces due to the tool-workpiece contact area reduction behind the tool tip (refer to Fig. 15(b)). Therefore, it is concluded that thrust force and induced damage are intimate related; the less thrust force is achieved, the less induced damage is obtained.

Relief angle 10° is found to reduce the damage for fibre orientations of 15°, 30° and 75° considerably. Besides, it is observed that relief angles of 8° and 10° minimised the induced damage in comparison with the rest of angles for 0° and 45° fibre orientations. For 60° fibre orientation, the relief angle effects are observed to be negligible and for 90° the relief angle of 6° a significant induce damage is achieved in comparison with the rest of angles simulated.

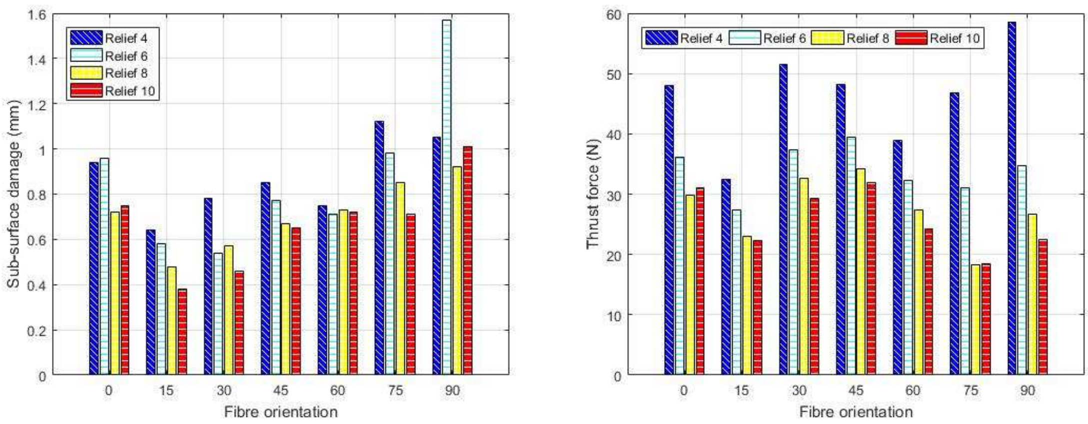

(a) (b)

Fig. 15. (a)Sub-surface damage and (b) thrust forces obtained for all the relief angles and fibre orientations studied at the final simulation time.

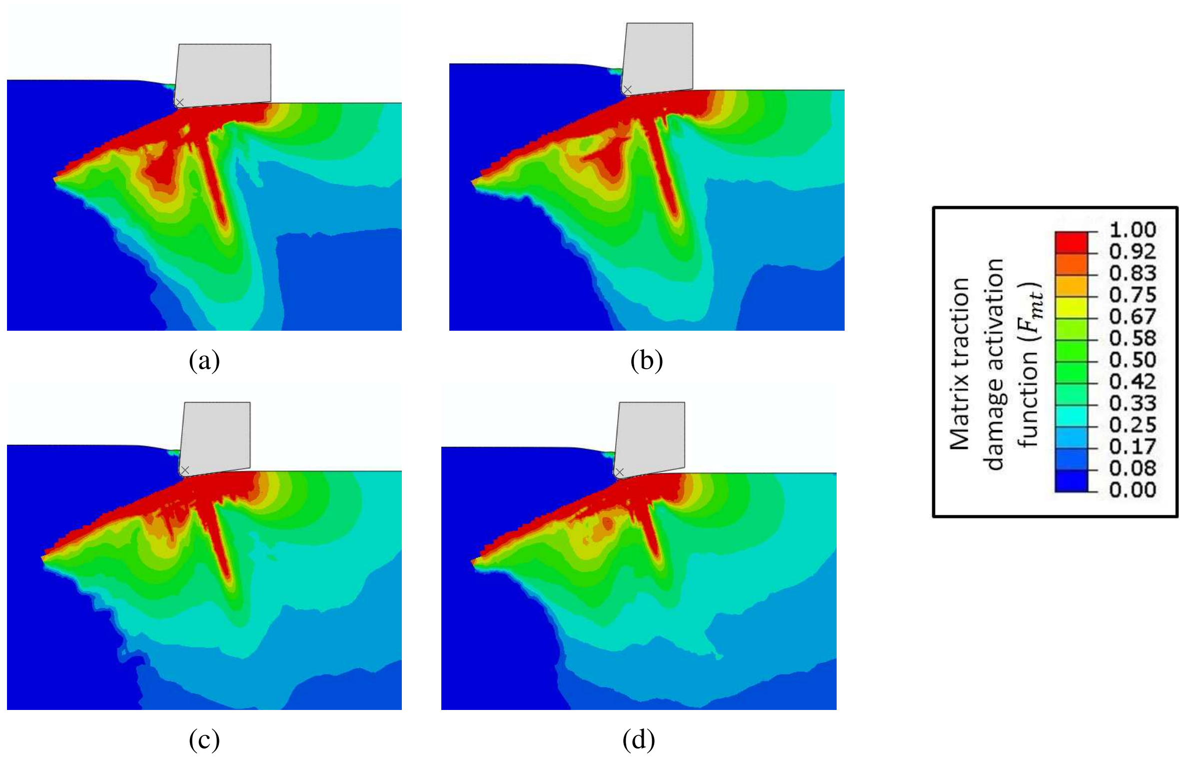

Fig. 16. F_{mt} obtained for relief angles (a) 4° (b) 6°, (c) 8° and (d) 10° at final simulation time for a fibre orientation of 75°.

It is appreciated that in the case of fibre orientations with 90° the results trend is not logic. For this particular case, the inclusion of an analysis of the fibre/matrix debonding could reflect better the tendency appreciated. This failure mechanism is not included in the current FE model and takes a relevant role for 90° and higher fibre orientations. The development of micro mechanical FE models with the implementation of cohesive properties between fibre and matrix are required to analyse this issue.

From the simulation results, it is observed that highest sub-surface damage exceeds more than 50% the lowest sub-surface damage for fibre orientations of 15°, 30°, 75° and 90°. Thus, it is concluded that the election of correct high relief angles is essential for not affecting the structural integrity of the laminate considerably. The factor F_{mt} is depicted in Fig. 16 for 75° fibre orientation to show the reduction of sub-surface damage with higher relief angles.

5.5. *Rake angle influence*

From the numerical results obtained in this work, not a clear rake angle tendency is observed to reduce the sub-surface damage. It is found that the rake angle which produced less sub-surface damage is fluctuating with the fibre orientation, see Fig. 17. Therefore, the best rake angle to reduce the level of damage in composite laminates should be analysed for each fibre orientation.

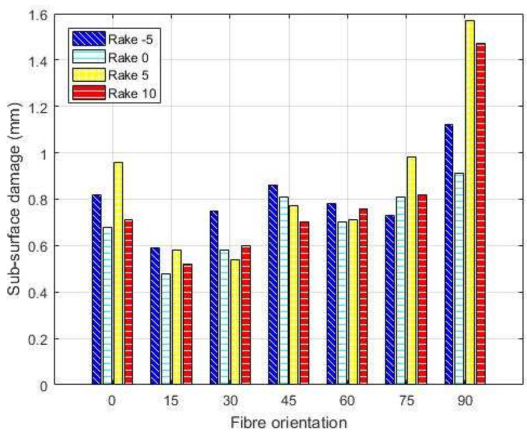

Fig. 17. Sub-surface damage obtained for all the rake angles and fibre orientations studied at the final simulation time.

Fig. 17 reveals that the rake angle of 0° obtains a low laminate induced damage for all fibre orientations. This rake angle is found to be the best machining option for fibre orientations of 0°, 15°, 60° and 90°. However, significant induced damage increments is not seen for fibre orientations between 0° and 75° which the maximum differences are around the 40%. Therefore, rake angle is considered not essential to reduce the remaining laminate damage in comparison with other cutting factors such us workpiece material or relief angle.

As shown in Fig. 17, rake angles of 5° and 10° are not a suitable solution for machining laminates with 90° as it produces higher damage levels. Finally, Fig. 18 represents the matrix compression activation function F_{mc} calculated at the final of the simulation for a fibre orientation of 30° as a mode of example.

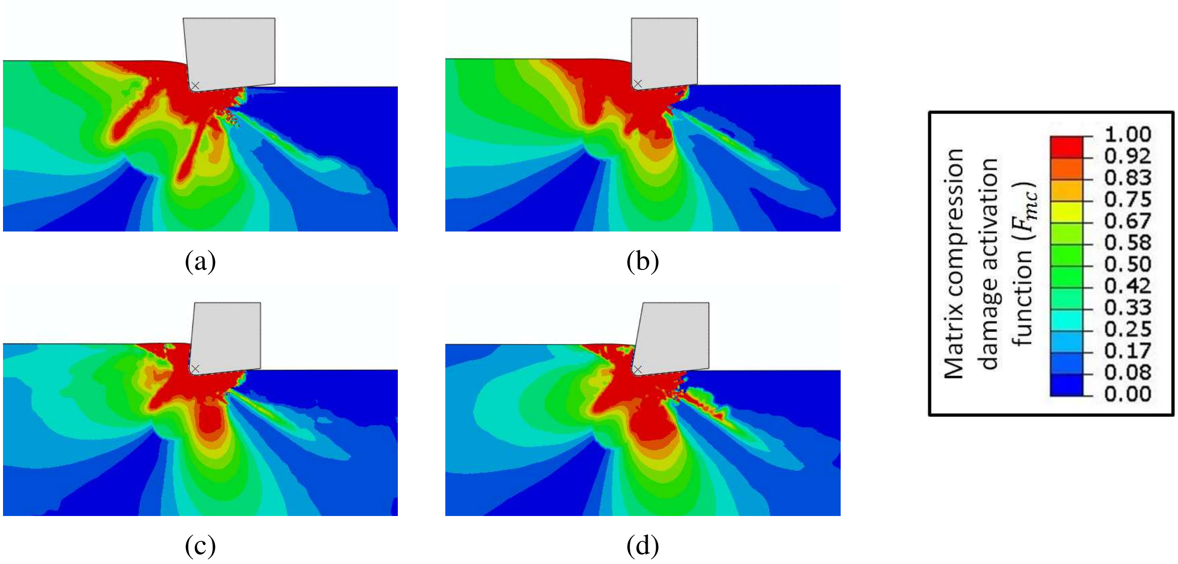

Fig. 18. F_{mc} obtained for rake angles (a) -5° (b) 0°, (c) 5° and (d) 10° at final simulation time for a fibre orientation of 30°.

6. Concluding remarks

This paper offers a novel orthogonal cutting FEM study of the effect of cutter parameters on machining induced damage. Spring back effect has been included adding a cutting tool vertical movement during the simulation improving the thrust force predictions. The use of a new damage algorithm composed of a linear stiffness degradation and a maximum damage limit for fibres and matrix has been demonstrated to improve previous sub-surface damage predictions. It has been demonstrated that matrix damage modes delimit the induced damage machining depth, distinguishing three main areas: (1) beneath, (2) behind and (3) in front of the cutting tool.

- Zone 1: Shear stress are predominant and as a result both matrix damages, cracking and crushing are developed.

- Zone 2: Cracking matrix mode is produced because of the tool-workpiece friction effect pull the material in this area.

- Zone 3: Crushing mode occurs due to the high compressive loads produce by the pushing action of the cutter tool.

Ten cutting configurations in relation to fibre orientation, material properties, edge radius, relief angle and rake angle, are simulated, concluding in the below statements.

- The low fibre orientations, i.e., 15° and 30°, show less induced damage than the higher fibre orientations, i.e., 75° and 90°. The low fibre orientations experiencing fragile chip ruptures, while higher orientations show more ductile chip rupture.
- The UD-CFRP composites experience more fragile chip fractures and provide much lower induced damages than the UD-GFRP composites for all fibre orientations. Machining forces are considerably higher for CFRP composites because its superior stiffness.
- In general, the tool wear effects do not generate high induced damage, with the exception of edge radius higher than 15 μm for 90° fibre orientation.
- High relief angles produce low sub-surface damages for all fibre orientations. It is noted that thrust forces are intimate related to the sub-surface damage observing that the less thrust force is achieved, the less induced damage is obtain.
- The rake angles studied does not affect considerably into the machining induced damage. The use of a rake angle of 0° is recommended to obtain lower induced damage levels on the laminate for every fibre orientation.

Acknowledgements

The first author wishes to acknowledge the financial support and technical help provided by the Industrial Doctoral Centre (IDC) of Sheffield and the Engineering and Physical Sciences Research Council (EPSRC) for making possible this paper.

The third author wishes to acknowledge the support by the Natural Science Foundation of Jiangsu Province (BK20180855) and China Postdoctoral Science Foundation (2018M640459).

References

[1] R. M'Saoubi, D. Axinte, S. L. Soo, C. Nobel, H. Attia, G. Kappmeyer, S. Engin, and W.-M. Sim, "High performance cutting of advanced aerospace alloys and composite materials," *CIRP Annals - Manufacturing Technology*, vol. 64, no. 2, pp. 557 – 580, 2015.

[2] J. Xu, A. Mkaddem, and M. El, "Recent advances in drilling hybrid FRP / Ti composite : A state-of-the-art review," *Composite Structures*, vol. 135, pp. 316–338, 2016.

[3] N. A. Abdullah, J. L. Curiel-Sosa, Z. A. Taylor, B. Tafazzolimoghaddam, J. L. Martinez Vicente, and C. Zhang, "Transversal crack and delamination of laminates using XFEM," *Composite Structures*, vol. 173, pp. 78–85, 2017.

[4] C. Zhang, J. L. Curiel-sosa, and T. Quoc, "Meso-scale progressive damage modeling and life prediction of 3D braided composites under fatigue tension loading," *Composite Structures*, vol. 201, no. June, pp. 62–71, 2018.

[5] J. L. Curiel-sosa, B. Tafazzolimoghaddam, and C. Zhang, "Modelling fracture and delamination in composite laminates : Energy release rate and interface stress," *Composite Structures*, vol. 189, no. January, pp. 641–647, 2018.

[6] O. Nixon-Pearson and S. Hallett, "An experimental investigation into quasi-static and fatigue damage development in bolted-hole specimens," *Composites Part B: Engineering*, vol. 77, pp. 462 – 473, 2015.

[7] R. Zitoune and F. Collombet, "Numerical prediction of the thrust force responsible of delamination during the drilling of the long-fibre composite structures," *Composites Part A: Applied Science and Manufacturing*, vol. 38, no. 3, pp. 858 – 866, 2007.

[8] C. R. Dandekar and Y. C. Shin, "Multiphase Finite Element Modeling of Machining Unidirectional Composites: Prediction of Debonding and Fiber Damage," *Journal of Manufacturing Science and Engineering*, vol. 130, no. 5, p. 051016, 2008.

[9] D. Nayak, N. Bhatnagar, and P. Mahajan, "Machining studies of ud-frp composites part 2: Finite element analysis," *Machining Science and Technology*, vol. 9, no. 4, pp. 503–528, 2005.

[10] G. Venu Gopala Rao, P. Mahajan, and N. Bhatnagar, "Machining of UD-GFRP composites chip formation mechanism," *Composites Science and Technology*, vol. 67, no. 11-12, pp. 2271–2281, 2007.

[11] K. A. Calzada, S. G. Kapoor, R. E. Devor, J. Samuel, and A. K. Srivastava, "Modeling and interpretation of fiber

orientation-based failure mechanisms in machining of carbon fiber-reinforced polymer composites," *Journal of Manufacturing Processes*, vol. 14, no. 2, pp. 141–149, 2012.

[12] G. V. G. Rao, P. Mahajan, and N. Bhatnagar, "Micro-mechanical modeling of machining of FRP composites - Cutting force analysis," *Composites Science and Technology*, vol. 67, no. 3-4, pp. 579–593, 2007.

[13] J. L. C. Sosa, N. Petrinic, and J. Wiegand, "A three-dimensional progressive damage model for fibre-composite materials," *Mechanics Research Communications*, vol. 35, pp. 219–221, 2008.

[14] J. L. Curiel Sosa, S. Phaneendra, and J. J. Munoz, "Modelling of mixed damage on fibre reinforced composite laminates subjected to low velocity impact," *International Journal of Damage Mechanics*, vol. 22, no. 3, pp. 356–374, 2013.

[15] C. G. Dávila, P. P. Camanho, and C. A. Rose, "Failure Criteria for FRP Laminates," *Journal of Composite Materials*, vol. 39, pp. 323–345, 2005.

[16] V. A. Phadnis, F. Makhdum, A. Roy, and V. V. Silberschmidt, "Drilling in carbon / epoxy composites : Experimental investigations and finite element implementation," *Composites Part A: Applied Science and Manufacturing*, vol. 47, pp. 41–51, 2013.

[17] G. V. G. Rao, P. Mahajan, and N. Bhatnagar, "Three-dimensional macro-mechanical finite element model for machining of unidirectional-fiber reinforced polymer composites," *Materials Science and Engineering A*, vol. 498, no. 1-2, pp. 142–149, 2008.

[18] S. Usui, J. Wadell, and T. Marusich, "Finite element modeling of carbon fiber composite orthogonal cutting and drilling," *6th CIRP International Conference on High Performance Cutting, HPC2014*, vol. 14, pp. 211–216, 2014.

[19] C. Santiuste, A. Olmedo, X. Soldani, and H. Migue, "Delamination prediction in orthogonal machining of carbon long fiber-reinforced polymer composites," *Journal of Reinforced Plastics and Composites*, vol. 31 (13), pp. 875–885, 2012.

[20] C. Santiuste, H. Miguélez, and X. Soldani, "Out-of-plane failure mechanisms in LFRP composite cutting," *Composite Structures*, vol. 93, no. 11, pp. 2706–2713, 2011.

[21] C. Santiuste, X. Soldani, and M. H. Miguélez, "Machining FEM model of long fiber composites for aeronautical components," *Composite Structures*, vol. 92, no. 3, pp. 691–698, 2010.

[22] S. Zenia, L. Ben Ayed, M. Nouari, and A. Delamézière, "Numerical analysis of the interaction between the cutting forces, induced cutting damage, and machining parameters of CFRP composites," *International Journal of Advanced Manufacturing Technology*, vol. 78, no. 1-4, pp. 465–480, 2015.

[23] X. Soldani, C. Santiuste, A. Muñoz-Sánchez, and M. H. Miguélez, "Influence of tool geometry and numerical

parameters when modeling orthogonal cutting of LFRP composites," *Composites Part A: Applied Science and Manufacturing*, vol. 42, no. 9, pp. 1205–1216, 2011.

[24] N. Bhatnagar, D. Nayak, I. Singh, H. Chouhan, and P. Mahajan, "Determination of machining-induced damage characteristics of fiber reinforced plastic composite laminates," *Materials and Manufacturing Processes*, vol. 19, no. 6, pp. 1009–1023, 2004.

[25] L. Lasri, M. Nouari, and M. El Mansori, "Modelling of chip separation in machining unidirectional FRP composites by stiffness degradation concept," *Composites Science and Technology*, vol. 69, no. 5, pp. 684–692, 2009.

[26] J. Xu and M. El Mansori, "Numerical modeling of stacked composite CFRP/Ti machining under different cutting sequence strategies," *International Journal of Precision Engineering and Manufacturing*, vol. 17, no. 1, pp. 99–107, 2016.

[27] J. Xu, M. El Mansori, and J. Voisin, "Numerical Modeling and FE Analysis of CFRP/Ti Stack Orthogonal Cutting," *Procedia CIRP*, vol. 46, pp. 67–70, 2016.

[28] R. Zitoune, F. Collombet, F. Lachaud, R. Piquet, and P. Pasquet, "Experiment-calculation comparison of the cutting conditions representative of the long fiber composite drilling phase," *Composites Science and Technology*, vol. 65, no. 3-4, pp. 455–466, 2005.

[29] C. Santiuste, J. Daz-lvarez, X. Soldani, and H. Migulez, "Modelling thermal effects in machining of carbon fiber reinforced polymer composites," *Journal of Reinforced Plastics and Composites*, vol. 33, no. 8, pp. 758–766, 2014.

[30] C. R. Dandekar and Y. C. Shin, "Modeling of machining of composite materials: A review," *International Journal of Machine Tools and Manufacture*, vol. 57, pp. 102–121, 2012.

[31] D. Che, I. Saxena, P. Han, P. Guo, and K. F. Ehmann, "Machining of Carbon Fiber Reinforced Plastics/Polymers: A Literature Review," *Journal of Manufacturing Science and Engineering*, vol. 136, no. 3, p. 034001, 2014.

[32] N. Shetty, S. M. Shahabaz, S. S. Sharma, and S. Divakara Shetty, "A review on finite element method for machining of composite materials," *Composite Structures*, vol. 176, pp. 790–802, 2017.

[33] I. Lapczyk and J. A. Hurtado, "Progressive damage modeling in fiber-reinforced materials," *Composites Part A: Applied Science and Manufacturing*, vol. 38, no. 11, pp. 2333–2341, 2007.

[34] M. J. Hinton, A. S. Kaddour, and P. D. Soden, "A comparison of the predictive capabilities of current failure theories for composite laminates , judged against experimental evidence," *Composites Science and Technology*, vol. 62, pp. 1725–1797, 2002.

[35] A. Puck and H. Schurmann, "Failure Analysis of Frp Laminates By Means of Physically Based Phenomenolog-

ical Models *," *Composites Science and Technology*, vol. 3538, no. 96, pp. 1633–1662, 1998.

[36] F. Paris, J. Cañas, and J. Marin, *Introduccion al analisis y diseño con materiales compuestos*. Sevilla: Universidad de Sevilla, Escuela Tecnica Superior de Ingenieros, 2008.

[37] C. Zhang, E. A. Duodu, and J. Gu, "Finite element modeling of damage development in cross-ply composite laminates subjected to low velocity impact," *Composite Structures*, vol. 173, no. 9, pp. 219–227, 2017.

[38] X. M. Wang and L. C. Zhang, "An experimental investigation into the orthogonal cutting of unidirectional fibre reinforced plastics," *International Journal of Machine Tools and Manufacture*, vol. 43, no. 10, pp. 1015–1022, 2003.